Molecular Dynamics Simulations of a Stretch-Activated Channel Inhibitor GsMTx4 with Lipid Membranes: Two Binding Modes and Effects of Lipid Structure

Manami Nishizawa and Kazuhisa Nishizawa
Department of Biochemistry, Teikyo University School of Medicine, Kaga, Itabashi, Tokyo 173-8605, Japan

ABSTRACT Our recent molecular dynamics simulation study of hanatoxin 1 (HaTx1), a gating modifier that binds to the voltage sensor of K^+ channels, has shown that HaTx1 has the ability to interact with carbonyl oxygen atoms of both leaflets of the lipid bilayer membrane and to be located at a deep position within the membrane. Here we performed a similar study of GsMTx4, a stretch-activated channels inhibitor, belonging to the same peptide family as HaTx1. Both toxins have an ellipsoidal shape, a belt of positively charged residues around the periphery, and a hydrophobic protrusion. Results show that, like HaTx1, GsMTx4 can interact with the membrane in two different ways. When all the positively charged residues interact with the outer leaflet lipid, GsMTx4 can assume a shallow binding mode. On the other hand, when the electrostatic interaction brings the positively charged groups of K-8 and K-28 into the vicinity of the carbonyl oxygen atoms of the inner leaflet lipids, the system exhibits a deep binding mode. This deep mode is accompanied by local membrane thinning. For both HaTx1 and GsMTx4, our mean force measurement analyses show that the deep binding mode is energetically favored over the shallow mode when a DPPC (dipalmitoyl-phosphatidylcholine) membrane is used at 310 K. In contrast, when a POPC (palmitooleoyl-phosphatidylcholine) membrane is used at 310 K, the two binding modes exhibited similar stability for both toxins. Similar analyses with DPPC membrane at 330 K led to an intermediary result between the above two results. Therefore, the structure of the lipid acyl chains appears to influence the location and the dynamics of the toxins within biological membranes. We also compared the behavior of an arginine and a lysine residue within the membrane. This is of interest because the arginine residue interaction with the lipid carbonyl oxygen atoms mediates the deep binding mode for HaTx1, whereas the lysine residue plays that role for GsMTx4. The arginine residue generally shows smoother dynamics near the lipid carbonyl oxygen atoms than the lysine residue. This difference between arginine and lysine may partly account for the functional diversity of the members of the toxin family.

INTRODUCTION

Mechanosensitive ion channels (MSCs) are integral membrane proteins that play a critical role in allowing a cell to sense physical forces within its environment (1). In eukaryotes, MSCs play a role in such important biological functions as hearing, touch, and cardiovascular regulation. The subtypes of MSC can be classified as stretch-activated channels (SACs) and stretch-inactivated channels.

A family of peptides has been discovered from the venom of the Chilean rose tarantula, *Grammostola spatulata*, which inhibit SACs in astrocytes and heart cells (2). GsMTx4 is the most potent of these toxins, selectively inhibiting the gating of cation selective channels and also exhibiting an effect at the cellular level that appears to involve the MSC activation (2). Of medical interest, GsMTx4 has been shown to inhibit atrial fibrillation potentiated by dilatation in the rabbit heart (3).

Structural studies show that GsMTx4 is a 34-residue cysteine knot peptide inhibitor with three disulfide bonds (4). GsMTx4, hanatoxin 1 (HaTx1, a gating modifier of K^+ channels), and several other peptide toxins constitute a peptide family in which several amino acid residues including the six cysteine residues are conserved (Supplementary Material Fig. S1). Fig. S1 focuses on the voltage sensor toxins and is based on the alignment shown in Lee and MacKinnon (5). (See Wang et al. (6) for SGTx1, Lee and McKinnon (5) for VSTX1, Middleton et al. (7) for ProTX2, and Escoubas et al. (8) for HmTx1 and ScTx1.) The six cysteine residues form a conserved motif, which is called an inhibitor cysteine knot (ICK) motif (9 and references therein). This structural motif is composed of an antiparallel, triple-stranded β-sheet stabilized by the cysteine knot. GsMTx4 and HaTx1 share an overall ellipsoidal shape, with a hydrophobic protrusion at the center and a belt (or ring) of positively and negatively charged residues around the periphery (Fig. 1; (4,10)).

Intriguingly, GsMTx4 and its enantiomer, enGsMTx4, exhibit similar efficacy in inhibiting SACs, suggesting that membrane distortion, rather than specific molecular recognition, is important for the function of GsMTx4 (11). The gramicidin A channels are dimers formed by the transbilayer association monomers in opposing monolayers (12). GsMTx4 causes a 10–25-fold increase in the channel appearance rate of gramicidin A and approximately a twofold increase in the open channel lifetime, leading the authors to conclude that GsMTx4 exerts its effect on the gramicidin A channel-formers by altering the lipid packing at the bilayer/solution/channel interface (11).

Submitted November 14, 2006, and accepted for publication February 12, 2007.

Address reprint requests to Kazuhisa Nishizawa, MD, PhD, Tel.: 81-3-3964-1211; Fax: 81-3-5375-6366; E-mail: kazunet@med.teikyo-u.ac.jp.

0006-3495/07/06/4233/11 $2.00

doi: 10.1529/biophysj.106.101071

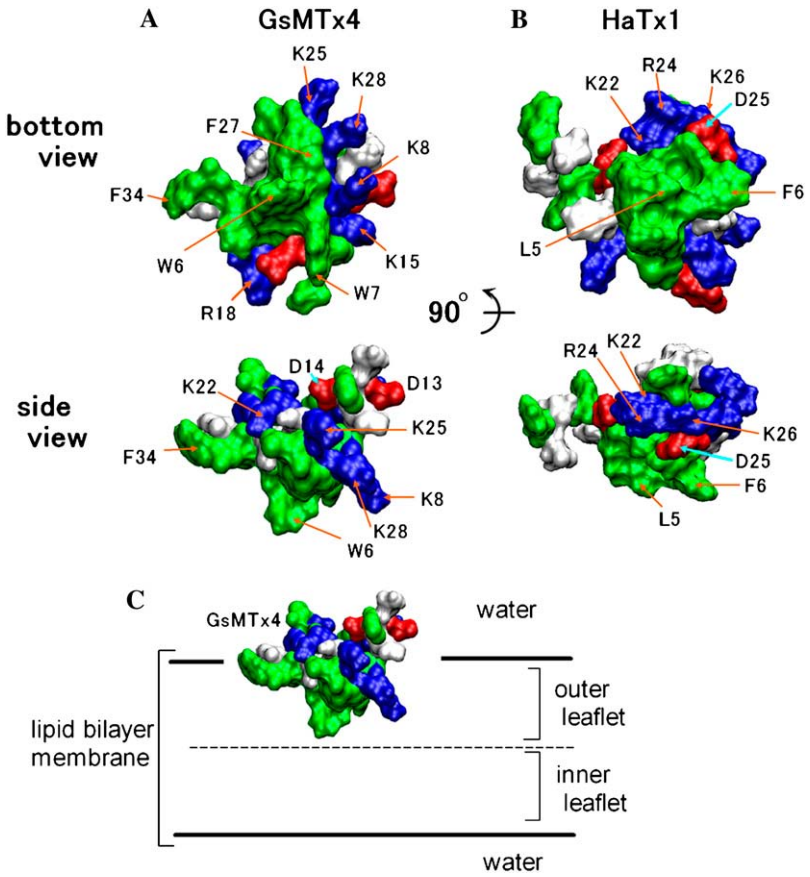

FIGURE 1 Surface structure of GsMTx4 and HaTx1. (*A* and *B*) The bottom and side views of the initial orientation used for simulations are shown for GsMTx4 (*A*) and HaTx1 (*B*). The orientation of GsMTx4 is represented as $(\theta_1, \theta_2) = (30°, -10°)$ using the angles as explained in the Simulation procedures section. The hydrophobic patch is oriented around the center of the normal view and at the bottom of the side view as described by Zhu et al. (9) and Takahashi et al. (10). Hydrophobic residues (Ala, Cys, Ile, Leu, Met, Phe, Pro, Trp, Tyr, and Val) are green, basic (Arg and Lys) are blue, and acidic (Asp and Glu) residues are red. Van der Waals surface structure was drawn using VMD (32). (*C*) Sketch showing the initial orientation of GsMTx4 relative to the bilayer membrane.

Molecular dynamics simulation is a well-established methodology for the study of the dynamics of proteins (13,14) and membranes (15). The treatment of lipid bilayer membranes has recently been improved, allowing systems involving increasingly complex proteins to be studied (e.g., 15–20). In our recent study, the positioning of HaTx1 in a lipid bilayer membrane was influenced by local (*cis*) and long-range (*trans*) interactions with the lipid headgroups (21). The long-range interaction is mediated by the side chains of R-24/K-26 and the carbonyl oxygen atoms of the inner (opposite) leaflet of DPPC (dipalmitoyl-phosphatidylcholine) of the membrane, bringing HaTx1 deep within the membrane. In our simulations, HaTx1 exhibits two modes of interaction with the DPPC bilayer membrane: the shallow mode and the deep mode. In the shallow mode, all the positively charged residues interact with the outer leaflet lipid, whereas in the deep mode, the electrostatic interaction brings the positively charged groups of R-24 and K-26 into the vicinity of the carbonyl oxygen atoms of the inner leaflet lipids. Only in the deep binding mode was the position of Trp-30 compatible with the experimental result of the fluorescence-quenching study by Phillips et al. (22), suggesting the biological relevance of the deep binding mode (21). It is still unclear as of yet whether the deep binding mode suggested for HaTx1 is also relevant for the other related peptides.

In this study, we conducted molecular dynamics simulations of GsMTx4 in DPPC and POPC lipid bilayer membranes. The membrane disordering, involving meniscus formation and the formation of hydrogen bonds between the lysine residues and the carbonyl oxygen atoms of the inner leaflet of the DPPC membrane, was observed as in the case with HaTx1. The different behaviors of HaTx1 and GsMTx4 in our simulations lead us to consider the physicochemical difference between the arginine and lysine residues during the interactions with membranes. We also report the difference between DPPC and POPC membranes, which demonstrates the influence of the lipid tail structure on the dynamics of the toxins.

Simulation procedures

In the following section, the term ''com'' indicates the center of mass. ''Bilayer center'' indicates the plane that is parallel to the membrane and contains the com of the membrane. The z axis is set to be parallel to the membrane normal.

Systems

The GROMACS 3.2.1 program (23,24) was used with the united-atom force field ffgmx (www.gromacs.org). For DPPC, the parameters modified by Tieleman and Berendsen (25)

were used. For POPC, the parameters provided by Dr. Tieleman's group as ''popc.itp'' at http://moose.bio.ucalgary.ca were used. For GsMTx4, we also tried the GROMOS96-43a1 parameter set (26) and found that the choice between ffgmx and 43a1 did not affect the overall results. For water, the SPC model was used (27). The bond lengths were constrained using LINCS (28). The cutoff for the Lennard-Jones interactions was set at 9 Å.

To account for the long-range electrostatic interactions under the periodic boundary condition, the particle mesh Ewald (PME) algorithm (29,30) was used with the real-space cutoff at 9 Å and the maximal grid size of 0.12 Å. The integration time step was set at 2 fs. The temperature was set at 310 K and 330 K (for DPPC) and 310 K (for POPC) with Berendsen coupling (31). The pressure was controlled by the Berendsen barostat at 1 atm with the independent (semiisotropic) coupling in the *xy*- and *z*-directions. From the bilayer of 128 DPPC molecules equilibrated by a 10-ns run starting with the coordinates obtained in our study (21), a DPPC bilayer, namely 61/61 (the number of DPPC molecules in the upper/lower leaflets), was prepared by removing six DPPC molecules (three from each leaflet of the membrane) located near the center of the membrane plane. This 61/61 was used for the embedding of the toxins. We also tested 60/64, but this alteration did not have a significant effect on the result.

The coordinates for GsMTx4 (1TYK) were obtained from the Brookhaven Protein Databank (4). To embed GsMTx4 into the membrane, SwissPDBviewer (us.expasy.org/spdbv) was used to remove molecular overlap. To keep the systematic bias minimal, only the minimally required horizontal movements of DPPC molecules away from the toxin were allowed. The distance between any atoms of DPPC and those of GsMTx4 was set at no less than 2 Å. The system was hydrated with 3660 water molecules containing 8 sodium and 12 chloride ions. HaTx1/DPPC simulations were performed as we described (21). A POPC (61/61) bilayer membrane was also prepared as in the case of the DPPC membrane.

When we carried out the 20-ns simulations of the pure membranes, under the PME treatment, all of the combinations, namely, DPPC/310 K, DPPC/330 K, and POPC/310 K, exhibited the features of the L_α state based on the lipid order parameter, the area per lipid, and the membrane thickness. On the other hand, under the cutoff method, only DPPC/310 K was clearly in the gel phase (Fig. S2 of Supplementary Material), whereas the other two combinations appeared to be in the L_α phase. Under the PME method, the area per lipid was ~67.2 and 70.7 $Å^2$ for DPPC/310 K and DPPC/330 K, respectively, whereas the corresponding values under the cutoff method were ~52.6 and 55.4 $Å^2$, respectively. Note that we use the PME method in this study.

Unless otherwise noted, after the energy minimization without constraints, an equilibration run was carried out for 1 ns constraining the GsMTx4 atoms, followed by a free 30-ns production run. Analysis of the properties of the system and movement of the toxin was done using a combination of GROMACS utilities and our own analysis programs. Calculations were carried out on 30 desktop PCs with 2.8-GHz processors with or without parallelization. All molecular images were made with Visual Molecular Dynamics (VMD) (32).

Energy analyses

We carried out the mean force measurement using the protocol described in Nishizawa and Nishizawa (21). Briefly, for the GsMTx4/DPPC analyses, the *z*-position of the com of the atoms belonging to either K-8 or K-28 of GsMTx4 was constrained and the force required for the constraint was measured using the ''constraints'' mode of the ''pull-code'' feature of GROMACS. We found it crucial to avoid the concerted movement of the lipid molecules close to GsMTx4, because such movement makes the meaning of ''the position within the membrane'' obscure. Therefore, we chose to harmonically restrain the *z*-coordinate of ''C-13'' of DPPC (C-13 is the atom that forms an O-ester with the *sn*-2 acyl chain) to avoid the gross deformation of the membrane during the preparation as well as the measurement. For the mean force measurement, the ''template frame'' was chosen from a trajectory exhibiting a mild but not intense membrane thinning. We chose the membrane for which the thickness of the part of the bilayer membrane containing GsMTx4 (i.e., the part consisting of the lipids whose *xy*-position is within ~0.6 nm of that of the GsMTx4 com) was ~2.4 nm based on the average distance of the C-13 atoms between the leaflets. We acknowledge that this choice had a shortcoming: the energy for the mild thinning (to 2.4 nm) must be taken into account. However, we can estimate the energy for the mild thinning of the membrane, so we revisit this point in the section for the mean force measurement.

We performed a 7-ns measurement of the force required for the constraint after the initial 2-ns equilibration run. For the HaTx1/DPPC study, the same procedure was performed, but the com of R-24/K-26 was constrained for the mean force measurement. For the toxin/POPC/310 K and toxin/DPPC/330 K analyses, the procedure was the same as toxin/DPPC/310 K, but the measurement periods were extended to 15-ns to cope with the relatively large fluctuations of the mean force. Qualitatively, the mean force measurement can be used for deriving the free energy profile, although in our case, the membrane fixation is artificial and the results should be carefully interpreted.

Azimuthal orientation

To indicate the orientation of GsMTx4 we defined two vectors: v_1 (the vector orienting from Cα of Cys-23 and ending at that of Asn-10) and v_2 (the vector from Cα of Cys-23 to that of Cys-30). Now the orientation of GsMTx4 is indicated by (θ_1, θ_2), where θ_1 is the angle between v_1 and the horizontal plane, which is perpendicular to the *z* axis, and θ_2 is that between v_2 and the horizontal plane. (The vectors are drawn in Supplementary Material Fig. S3.)

RESULTS AND DISCUSSION

The overall folding of GsMTx4 and HaTx1 has been shown to be similar (4,10): an ellipsoidal shape with a hydrophobic protrusion as well as positively or negatively charged residues forming a ring (or belt) around the periphery (Fig. 1). Of interest, the ''belt of the positively charged residues'' of GsMTx4, consisting of K-8, K-28, K-25, and K-22, lies in an oblique fashion (with K-8 at a low and K-22 at a high position) when the hydrophobic protrusion is placed downward. This is different from HaTx1, where the belt is horizontal when oriented similarly (Fig. 1 *B*). Under the default condition of the protonation at pH 7.5, the total net charge of GsMTx4 is +4e (one Glu-, two Asp-, six Lys-, and one Arg residue), whereas that of HaTx1 was +2e.

In the following, we mainly show the results for the system GsMTx4/DPPC/310 K because this allows a comparison with our recent study (21). The results of the other systems (i.e., the toxin/DPPC/330 K, toxin/POPC/310 K) are given briefly in the section describing the mean force measurement. For the first set of simulation analyses, the orientation shown in Fig. 1 *A* ($(\theta_1, \theta_2) = (30°, -10°)$) was used as the initial coordinate, i.e., with the hydrophobic protrusion facing the hydrophobic interior of the DPPC bilayer membrane. The position of the GsMTx4 com from the bilayer center was varied by a 0.25-nm step in the range from 0 nm to 1.75 nm. We named these simulations sim-0, -025, -05, -075, -10, -125, -150, and -175, where the number corresponds to the initial composition.

Transbilayer coupling

The movement of the GsMTx4 com exhibited one of the two alternative patterns, depending on its depth in the initial configuration (Fig. 2). When GsMTx4 was placed at deep positions (the com 0–0.75 nm above the bilayer center), the com moved to a point ~0.7 nm above the bilayer center within the initial ~5 ns. When the initial position of the GsMTx4 com was 1–1.75 nm above the bilayer center, the com position converged to a point ~1.4 nm above the bilayer center. Upon convergence, these com positions (i.e., 0.7 and 1.4 nm above the bilayer center) corresponded to two different modes of interactions, what we call the deep mode and shallow mode, respectively. Fig. 3 shows representative snapshots from sim-05, which converged to the deep mode. The deep mode was accompanied by membrane deformation: outward translocation of several inner leaflet DPPC molecules and their interaction with the side chain of one or two lysine residues, typically, K-8 and K-28.

In the shallow binding mode, the positively charged residues were located near the headgroup of the outer leaflet DPPC (Supplementary Material Fig. S3 *b*) and interacted with the carbonyl oxygen atoms or the water molecules that penetrated from the outside. Whereas in the deep binding mode, the positively charged residues split into two groups,

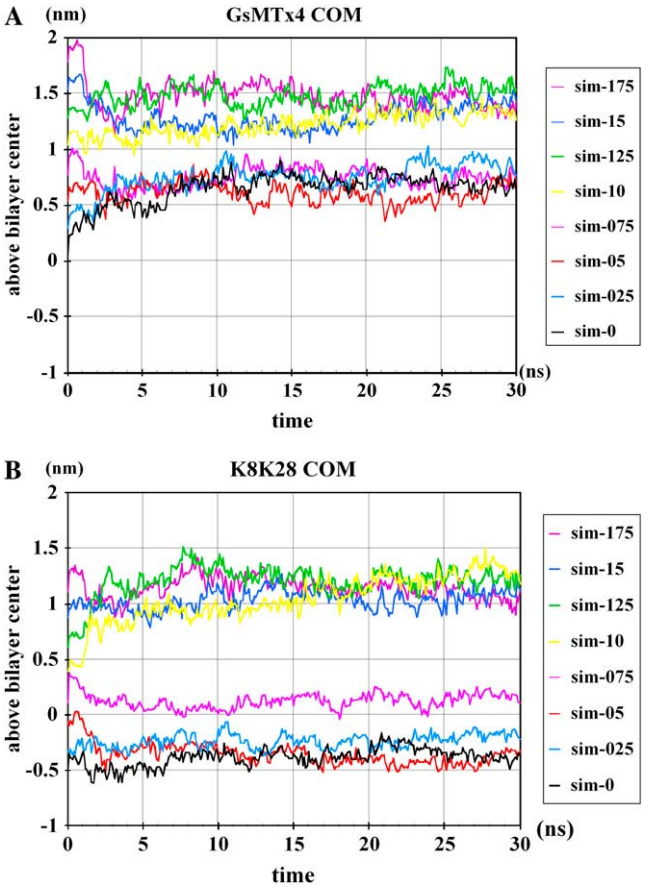

FIGURE 2 (*A*) Time course of the position of the GsMTx4 com for the simulation runs (sim-0–175). Each curve corresponds to a simulation, for which the initial GsMTx4 com position (nanometer above the bilayer center) is indicated by a number: 0, 0.25, . . . , or 1.75. Sim-075 (*curve* ''0.75'', with the same color as ''1.75'') exhibited the deep binding mode, like three other simulations, i.e., ''0'', ''0.25'', and ''0.5'' nm. (*B*) Same as in *a* but the time course of the composition of K-8/K-28 is shown.

each interacting with the outer and inner leaflet carbonyl groups (Fig. 3). The two binding modes are also evident from the time course of the com position of K-8/K-28 (Fig. 2 *B*). When the initial position of the com of GsMTx4 was shallow (1–1.75 nm above the bilayer center), the com of K-8/K-28 was directed to the carbonyl oxygen layer, whereas when the initial position was deep (com 0–0.75 nm above bilayer center) the position of the K-8/K-28 com remained near the depth of the bilayer center. For sim-075, the K-8/K-28 com stayed in a position slightly higher than for sim-0–05, but we confirmed that the side chains of K-8 and K-28 were interacting with the carbonyl oxygen atoms of the membrane inner leaflet. K-15, K-22, and K-25 were always bound to the outer (upper) leaflet in both deep and shallow binding modes.

As Fig. 3 suggested, the GsMTx4-induced membrane deformation was uneven around GsMTx4 in cases exhibiting the deep mode interaction; the inner leaflet lipids located near K-8/K-28 exhibited a marked outward translocation compared with the inner leaflet lipids near the other residues of

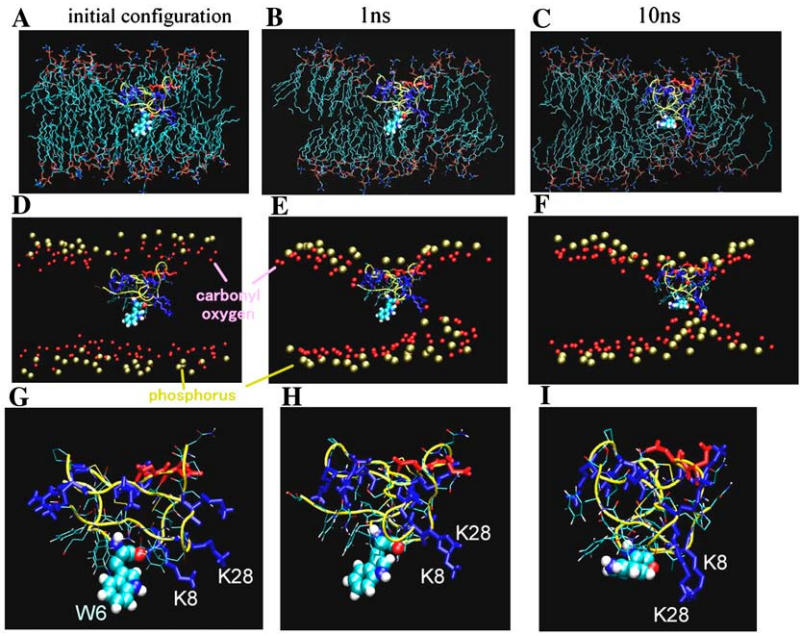

FIGURE 3 Snapshots taken from representative trajectories. (*A–C*) Snapshots at the indicated time points of the sim-05. For clarity, only the nonwater atoms contained in a slice of 3-nm thickness are shown. The peptide backbone is shown as a yellow tube. (*D–F*) The same as in *A–C*, respectively, but a different representation. The phosphorus atoms of DPPC are shown as ocher spheres. DPPC acyl chains are not shown. Trp-6 is shown by light blue and white spheres. Charged residues are shown as a blue (Arg, Lys) or red (Asp, Glu) licorice. (*G–I*) The same as *A–C*, respectively, but feature GsMTx4 with similar presentation to (*D–F*) but showing the peptide only.

GsMTx4. This is confirmed in Fig. 4, where the density of each atom of the lipids belonging to the space defined by a large y component of the coordinate ($4.2 < y < 5.2$ nm) is shown in comparison with that of the lipids belonging to the $3.2 < y < 4.2$ nm area. For sim-05 (the deep binding mode, Fig. 4 *B*), with $4.2 < y < 5.2$ nm, which contains K-8/K-28, the lipid headgroups of the inner membrane leaflet were significantly translocated outward (i.e., rightward of the graph), whereas in the $3.2 < y < 4.2$ nm area, the lipid headgroups of the inner membrane leaflet were found at a level similar to the case with the shallow mode (the sim-150, Fig. 4 *A*).

For the outer leaflet, the asymmetry between the two areas (i.e., with $4.2 < y < 5.2$ and $3.2 < y < 4.2$) was insignificant for the shallow mode (Fig. 4 *A*). In contrast, in the deep mode (sim-05, Fig. 4 *B*), the area with $4.2 < y < 5.2$ nm of the outer membrane showed an inward translocation of DPPC molecules (i.e., a leftward shift) compared to the shallow mode, showing the intense outer leaflet deformation for the deep binding mode (Fig. 4 *B*). We frequently found that in the deep binding mode several lysine residues including K-15 and K-25 acted to draw the outer leaflet lipids inward, whereas K-8 and K-28 persistently interacted with the inner leaflet (details not shown). To summarize, the deep binding mode was accompanied by an intense membrane deformation and the degree of deformation was greater for the area with $4.2 < y < 5.2$ nm, which contains K-8/K-28. Therefore, the part of GsMTx4 that contains K-8/K-28 acts to draw both leaflets of the membrane closer to each other in the deep binding mode but not in the shallow mode.

The conformational stability of GsMTx4 was assessed by measuring the conformational drift, as given by the Cα atom root mean-square deviation (RMSD), from the initial structure. To summarize the results, besides both termini (G-1 and F-34), the structure of the two loops, P-11-D-14 and K-25-F27, in our simulations were slightly different from the NMR-determined structure, but the difference is small, with an RMSD in the range 0.2–0.3 nm. The RMSD relative to the structure found in the middle of the simulations was smaller for the deep mode (0.065 nm) than for the shallow mode (0.081 nm) and the water (0.12 nm), suggesting that movements of the Cαs were most strongly suppressed in the deep mode. As these values showed, the overall structure of GsMTx4 was stable. We did not observe any gross deformation of GsMTx4 during the simulations.

Membrane deformation

In all the simulation runs exhibiting the deep binding mode (sim-0–sim-075), intense membrane deformation was observed as shown in Fig. 3. Fig. S4 shows the positions of C-13 (the carbon atom that forms an O-ester with the *sn*-2 acyl chain) of those DPPC molecules which were located within the vertical cylinder with a radius of 1.3 nm from the GsMTx4 com. Typically, the intense membrane thinning associated with the deep mode was completed within the initial 1 ns; the DPPC molecules of the inner leaflet moved upward, and the outer leaflet DPPC molecules in the proximity of GsMTx4 moved inward, creating a meniscus. In all such cases, the hydrogen bonds between the carbonyl oxygen atoms and amide groups of K-8 and K-28 were observed. Fig. 5 shows the number of hydrogen bonds between K-8/K-28 and DPPC oxygen atoms as well as water oxygen atoms for the sim-05. The number of hydrogen bonds between K-8/K-28 and water molecules was small (~five or fewer) for all the trajectories. The total number of hydrogen bonds was basically similar between the two binding modes, and therefore the number of

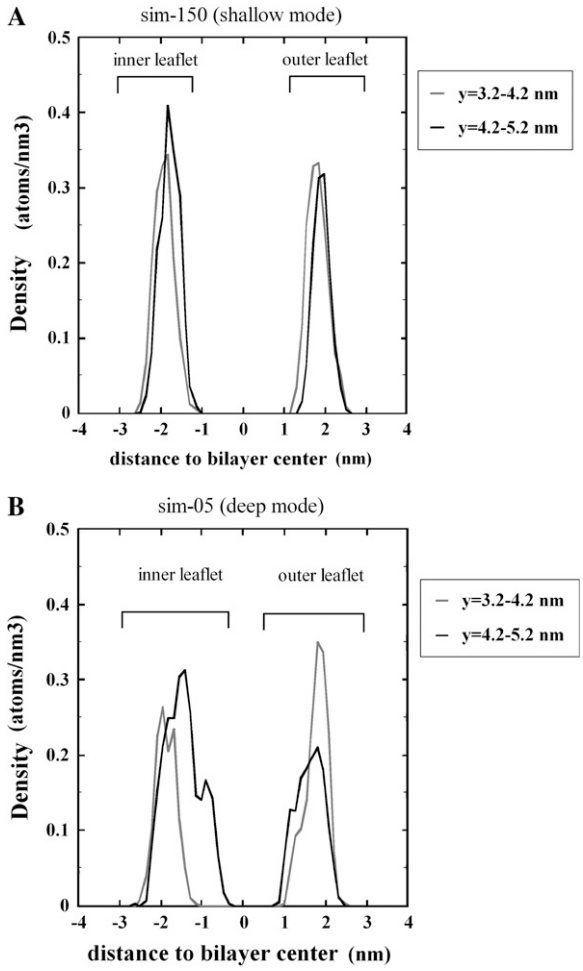

FIGURE 4 Density of phosphorus atoms of DPPC plotted against the z-component of the coordinate. (*A*) The result for sim-150 is shown. (*B*) The result for sim-05 is shown. For the inner leaflet ($z = 0$–~ 3), asymmetry is evident with respect to the y-component of coordinates. That is, for DPPC molecules belonging to the slice of $y = 4.2$–5.2, the inner leaflet lipids translocated outward (i.e., to the area with greater z-component).

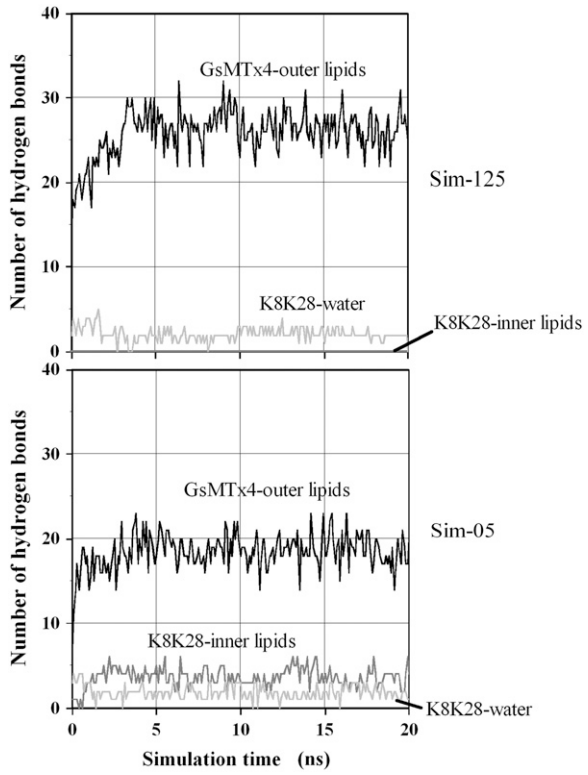

FIGURE 5 Number of hydrogen bonds plotted versus simulation time. Hydrogen bonds between GsMTx4 and the outer leaflet of the membrane are shown in dark gray, whereas those between K-8/K-28 and the inner leaflet lipids are shown in black. Hydrogen bond between K-8/K-28 and water molecules are shown in light gray. (*Top*) The result for a trajectory exhibiting the shallow mode (sim-125). Note that in the shallow mode, no hydrogen bond was formed between K-8/K-28 and the inner leaflet lipids. (*Bottom*) The result for the deep mode (sim-05).

hydrogen bonds is not likely to account for a substantial part of the energy difference between the modes.

The deep binding mode was accompanied by membrane deformation where several water molecules penetrated from the inner (lower) water layer and usually were associated with the charged residues (Fig. S5). The outer and inner bulk water layers approached but remained more than 1.4 nm away.

Fig. 6 illustrates how GsMTx4 affects the lipid diffusion, by plotting all the (x,y) coordinates of the phosphorus atoms during the 20–30-ns period. GsMTx4 in the shallow binding mode significantly decreased the free motion of the lipids of the outer (*cis*) but not the inner leaflet of the membrane. By contrast, GsMTx4 in the deep binding mode decreased the motion of the lipids for both the outer and the inner leaflet of the membrane.

We also performed simulations with varied initial orientations of GsMTx4. Both θ_1, θ_2 were varied over the range of from $+40°$ to $-40°$, and the GsMTx4 com position was placed at either 0.25 nm or 1.25 nm above the bilayer center. The results were similar to the above ones; the simulations starting with deep GsMTx4 position exhibited reorientation and converged to the deep mode with $(\theta_1, \theta_2) = \sim(-15°, 30°)$, whereas those with a shallow GsMTx4 position converged to the shallow mode with $\sim(10°, -30°)$ (data not shown). In all cases, reorientation took ~20–30 ns depending on the initial orientation. All the trajectories starting with the GsMTx4 com at 0.25 nm above the bilayer center resulted in the splitting of the positively charged residues into two groups, those interacting with the outer leaflet and those interacting with inner leaflets. In one case, K-25/K-28 instead of K-8/K-28 interacted with the inner leaflet of the membrane (not shown). Hence, the specificity of the residues that interact with the inner leaflet lipid seems somewhat arbitrary.

Long-range electrostatic interaction necessary for membrane deformation

In the case of HaTx1, the long-range electrostatic interaction between R-24/K-26 and the inner leaflet DPPC was

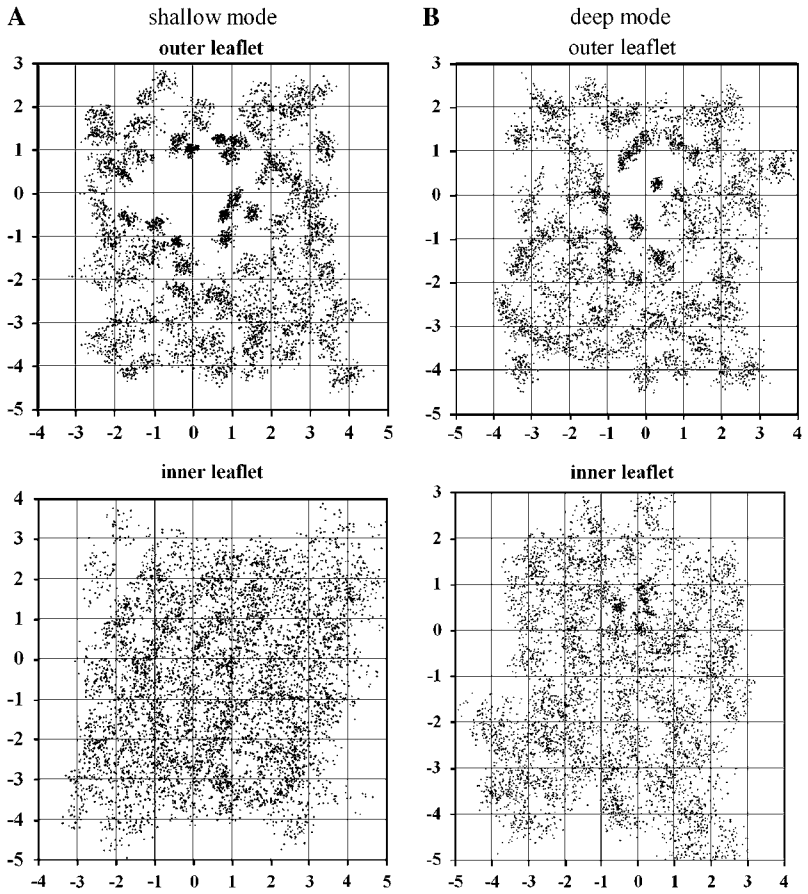

FIGURE 6 Distributions of phosphorus atoms during 10–20 ns of simulation. (*Top*) The outer leaflet; (*bottom*) the inner leaflet. Shown are the data from 100 frames covering 10–20 ns of simulations. These are raw frames and they were not centered around peptide. Therefore, the data include the diffusion of both the peptide and DPPC molecules. (*A*) Shallow binding mode. (*B*) Deep binding mode.

necessary for the deep binding and the resultant membrane thinning (21). When we used a cutoff method, instead of the PME method, such that the long-range electrostatic interactions between GsMTx4 and the polar headgroups of the inner leaflet are turned off, the membrane deformation was abolished, indicating that the long-range electrostatic attraction is necessary for the membrane deformation (data not shown). To examine the robustness of this deformation, we reduced the atomic charges assigned to the 10 DPPC molecules' carbonyl oxygen atoms. By downscaling by multiplication by 0.2, the membrane deformation was still observed. However, this deformation was abolished using the 0.8-nm cutoff, indicating that despite the reduced atomic charges of the carbonyl oxygens, the electrostatic interaction causes the membrane deformation.

When the net charge of K-8 and K-28 was nullified by deprotonation, neither the membrane deformation nor the inward movement of K-8 and K-28 was observed, although the same initial coordinates as sim-05 were used (''n-05'' of Fig. S4). The com of K-8/K-28, which was initially 0.5 nm above the bilayer center, gradually moved upward and reached the level of the carbonyl oxygen atoms of the outer leaflet of the membrane at ~20 ns (Fig. S4 *bottom*, *green line*). Therefore, the membrane thinning is caused at least in part by the electrostatic attractive force between the positively charged side chains of K-8 and K-28 and the carbonyl oxygen atoms of the inner leaflet.

Two binding modes: mean force measurement analyses with DPPC and POPC membranes

In the case of HaTx1 within the DPPC membrane, our simulation suggested that the deep mode was more energetically favorable than the shallow mode and the deep mode, but not the shallow mode, places W-30 at a position consistent with the experimental findings (21). Although a spectroscopic analysis of GsMTx4 in the membrane has not been done to our knowledge, it seems worthwhile to compare HaTx1 and GsMTx4 in terms of the energy governing the relative stability of the modes. As a first step to approximate the free energy evaluation, we chose the mean force measurement using the constrained membrane. This approach is based on the measurement of the force required to restrain the *z*-directional movement of the K-8/K-28 com. The measurement was carried out under the condition of membrane fixation (constraining the *z*-position of C-13 of DPPC molecules) to avoid the concerted movement of DPPC, which makes the discrimination of the two binding modes difficult. As we commented in the Simulation procedures section, we used the template frame, which was the membrane with a mild thinning

and which allowed both the deep and shallow binding modes, and it was therefore necessary for us to compare the two modes. The energy cost for this thinning is estimated in the legend for Supplementary Material Fig. S6.

Fig. 7 *A* shows the result compared to HaTx1 (21). Because the mean force was negligibly small (<0.6 kJ/nm/mol) when the com of K-8/K-28 (for GsMTx4) and of R-24/K-26 (for HaTx1) was set at 4 nm above the bilayer center, the position 4.125 nm above the bilayer center was used as the reference point for the free energy profile. For both toxins, the shallow and deep modes were observed when the com was ~1.5 nm and −0.5 nm from the bilayer center, respectively. For GsMTx4, the free energy of the deep mode was ~125 kJ/mol lower than the shallow mode. This value is comparable to the value obtained for HaTx1 (~115 kJ/mol).

To gain insight into the effect of the acyl chain structure of the membrane lipid on the dynamics of the toxins, we extended our analyses to the POPC/310 K bilayer membrane. Free simulation runs showed that, for both HaTx1 and GsMTx4, the deep and shallow modes are possible with the POPC membrane, but only those simulations with a fairly deep initial com position (at least −0.5 nm from the bilayer center) resulted in the deep binding mode (details not shown), suggesting that the ''basin'' for the deep binding mode is not as wide as in the cases with the DPPC membrane. Consistent

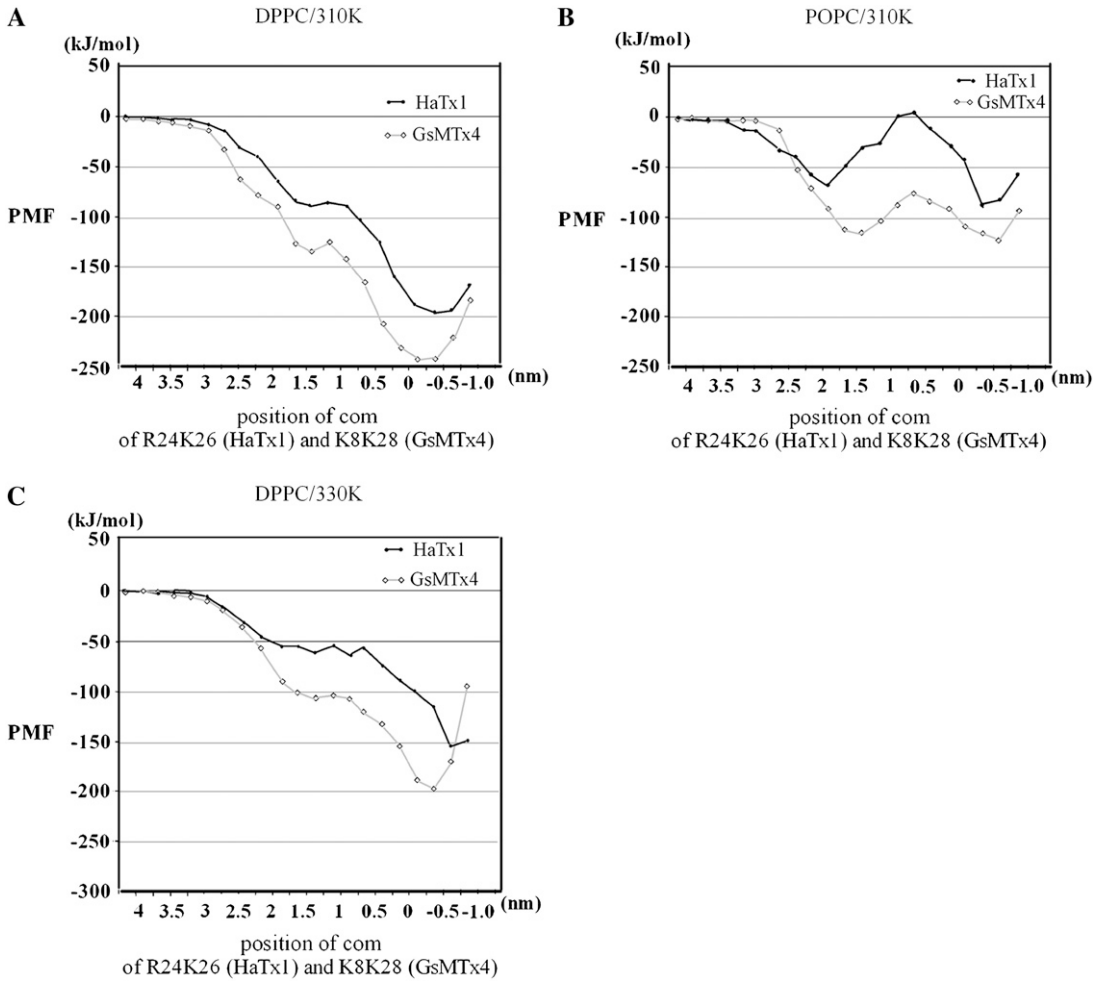

FIGURE 7 Free energy profile for K-8/K-28 (GsMTx4) and for R-24/K-26 (HaTx1) obtained by the mean force measurement. (*A*) Results with the DPPC/310 K membrane. (*B*) Results with the POPC/310 K membrane. (*C*) Results with the DPPC/330 K membrane. The free energy profile was derived from simple integration of the mean force acting on K-8/K-28 and R-24/K-26, which was constrained at various positions. As noted in the Simulation procedures section, we chose a coordinate set as the template frame and therein restrained the *z*-coordinates of ''C-13'' of DPPC and POPC (C-13 forms an O-ester with the *sn*-2 acyl chain). For the analyses shown here, the thickness of the proximal part of the membrane was 2.4 nm based on the average positions of the C-13 atoms. We utilized the pull-code feature of GROMACS to constrain the *z* axis movement of the RK- or KK-group for a 7-ns measurement of the force required for the constraint after the initial 2-ns equilibration run. For the POPC/310 K and DPPC/330 K analyses, we typically extended each productive run to 15 ns because the mean force showed a fluctuation on a scale of ~2–3 ns. To accommodate the toxins in the simulation box, the size of the box in *z*-direction was lengthened to 7.2, 7.5, 8.0, and 8.5 nm, respectively, for the measurement with the com 2.5, 3.0, 3.5, and 4.0 nm above the bilayer center, respectively. For these com positions, the number of water molecules was also increased up to 3970, 4560, 4956, and 5729, respectively, by introducing extra water molecules.

with this, the mean force measurement for GsMTx4 showed that the shallow binding mode was similarly favored as the deep binding mode (Fig. 7 *B*). In the case of HaTx1, the deep binding mode was favored over the shallow binding mode, but the difference in energy between the two modes was small (~20 kJ/mol).

These findings show that the presence of the unsaturated bonds within the lipid acyl chains causes the instability of the deep binding mode relative to the shallow mode. Another feature of the POPC membrane is that, unlike the case with the DPPC membrane, the energy barrier between the two binding modes was high: 60 kJ/mol for HaTx1 and 40 kJ/mol for GaMTx4. Although it is speculative, these findings along with our visual inspection lead us to surmise that the POPC membrane does not accommodate the toxins in the deep position as well as the DPPC membrane because the cone-like shape of a POPC molecule tends to ''expel'' the toxins to the membrane surface. When we performed a similar set of analyses with the DPPC/330 K membrane, we found that whereas GsMTx4 exhibited a PMF profile similar to that obtained with DPPC/310 K, the profile for HaTx1 was somewhat alike that obtained for HaTx1/POPC/310 K (Fig. 7 *C*). Although these results may be caused by the difference in fluidity among the membrane/temperatures and although the fluctuations of the mean force data were not very large (Supplementary Material Fig. S6), it is currently difficult to consider the difference between GsMTx4 and HaTx1 and the difference among the DPPC/310 K, DPPC/330 K, and POPC/310 K to be statistically significant because our simulation time is extremely limited.

We note that the results (and our impressions as well) do not show that the shallow binding to the POPC/310 K membrane is more favorable than the shallow binding to the DPPC/310 K membrane. Intriguingly, if we assume that the reference points (i.e., the *leftmost point*) of Fig. 7, *A* and *B*, have a common free energy value, then the results imply that the shallow binding to the POPC membrane is largely as favorable as that to the DPPC/310 K. It seems possible that for both toxins, the deep binding to the DPPC/310 K membrane has a greater binding energy than the shallow binding to the POPC/310 K membrane.

However, because our analyses are far from the exhaustive and cell membranes contain various components including cholesterol and sphingomyelin, it is currently difficult to consider the relevance of these findings to real cell membranes. It may be worthwhile to remember the experimental findings showing the unusually long delay (approximately minutes) before the action of these toxins, suggesting the presence of a high energetic barrier to the site of the action (11,22,33). Because our analyses show that deep binding to the DPPC membrane was more favorable than shallow binding to the POPC membrane, it is tempting to envisage that HaTx1 and GsMTx4 may seek out the lipid molecules with saturated acyl chains and ''create'' a domain rich in saturated lipids around themselves. However, it should be noted that our measurements were done only on an extremely short timescale relative to lipid degrees of freedom and in particular the motion of the toxin within the membrane.

It is important to note that many membrane processes happen at mesoscopic length- and timescales—that is, above 10–1000 nm and 10–1000 ns, respectively—and involve the collective nature of the system. Lateral movement of lipids by diffusion within membranes over several nanometers is a process requiring time on a scale of 100 ns. Diffusion and rotation of small proteins within lipids can also be considered to occur on scales above ~100 ns. Furthermore, in our simulations, the restraints introduced to the lipids and peptide should make these processes even slower. Therefore, the results shown in Fig. 7 are not conclusive and it is possible that much longer simulations nullify the difference between the membrane/conditions.

Smoothing effect of R as opposed to K on the peptide movement within the membrane

Although the general feature of the peptide-lipid interaction was similar between HaTx1 and GsMTx4 in our simulations, we empirically noted that it was relatively easy to move HaTx1 from one mode to another, but it was difficult to detach the positively charged residues of GsMTx4 from the lipid headgroups after one of the binding modes was established (M. Nishizawa and K. Nishizawa, unpublished results). We reasoned that this difference may be partly due to the fact that for HaTx1 one arginine as well as one lysine residue mediate the deep mode, whereas for GsMTx1, two lysine residues mediate the deep mode. Contrary to lysine, where the +1e charge is confined to an amino group, arginine's +1e charge is dispersed over the guanidinium group. This delocalization of charge may enable the arginine residue to capture undulations, on a relatively wide scale, of the electrical field rather than very local undulations.

To gain more insight, we carried out a steered molecular dynamics procedure using the peptides Ace-R-NH_2 and Ace-K-NH_2, where Ace is an acetyl group with a membrane consisting of 32(outer)/32(inner) DPPC molecules. Each of the amino acids was placed within the headgroups of the outer leaflet lipids, and the com of the side chain of the amino acid was pulled inward. Our anticipation was that, as the amino acid travels inward, the lipids which initially interacted with the amino acid should detach from the amino acid and the inner leaflet lipids should begin to interact in place.

As compared to Ace-K-NH_2, it was easier to detach Ace-R-NH_2, from the carbonyl and phosphate oxygen atoms of the outer leaflet by the inward vertical pulling (Fig. 8; in this figure, the ordinate represents the number of the interacting atoms of the lipids; the abscissa is the simulation time, which is effectively equivalent to the position of the com of the amino acid side chain because a stiff spring was used for the pulling). In fact, in the case of Ace-R-NH_2, the outer leaflet DPPC molecules interacting with Ace-R-NH_2 were typically

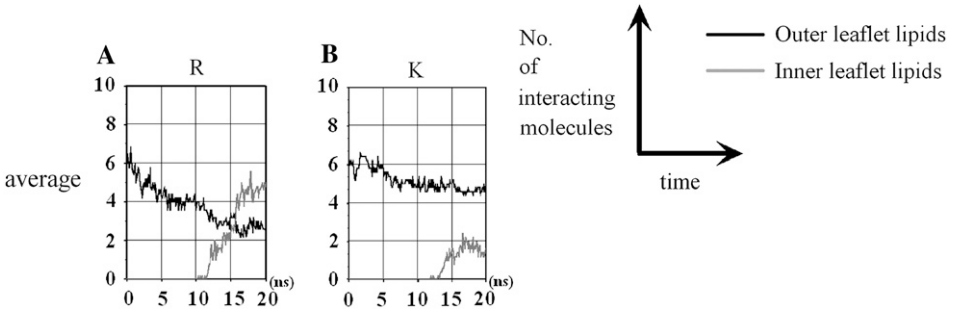

FIGURE 8 Steered molecular dynamics analysis with Ace-R-NH_2 and Ace-K-NH_2. (*A*) The number of lipid atoms interacting with Ace-R-NH_2 represented as a function of the simulation time. Shown is the average of five independent simulations. A ''stiff'' spring (the force constant of the spring was set at 5000 kJ/nm^2/mol) was used to pull the com, so that the simulation time largely reflects the position of the com of the amino acid side chain. Here, the ''interacting atoms'' were defined as the atoms being within 0.6 nm of the com of the arginine side chain. At most, only one atom per ''charge group'' of the force fields was counted because, for example, the two oxygen atoms of the same acyl chain behave in a correlated manner. The com of Ace-R-NH_2 was pulled inward after a 1-ns equilibrium run at the depth of 2.25 nm above the com of the reference group, i.e., the group of C-13 atoms of the inner leaflet lipids located outside the 1.5-nm-diameter cylinder and within the 3.0 nm diameter cylinder. Here both cylinders are defined to be centered on the com of Ace-R-NH_2 and oriented in parallel with the membrane normal. The pulling was performed at the rate of 0.1 nm/ns with respect to the distance between the coms of Ace-R- NH_2 and the reference group. (*B*) Same as in *A*, but the results with Ace-K-NH_2 are shown. For both *A* and *B*, the average of five independent simulations is shown.

replaced by inner leaflet DPPC molecules when Ace-R-NH_2 was at the depth of 0.5 nm below the bilayer center, whereas in the case of Ace-K-NH_2, only a limited number of such molecules was replaced by the inner leaflet DPPC molecules even at the end of the trajectory, when the Ace-K-NH_2 was 1 nm below the bilayer center, which is almost as deep as the original inner leaflet carbonyl oxygen layer. In addition, the force required to pull inward Ace-R-NH_2 was significantly smaller than that required for Ace-K-NH_2 (M. Nishizawa and K. Nishizawa, unpublished results).

It is well known that the basic residues on the voltage-sensor of the voltage-dependent ion channels are nearly always arginine, not lysine (for example, 34). Intriguingly, it has been proposed that the diffuse positive charge on the guanidinium group of arginine may make the transfer from water to lipid energetically less costly than with lysine (34). Four arginine residues are present on the same side of the S4 helix of KvAP and Kv1.2 channels (34,35). It is tempting to envisage that, when the electrostatic energy drives the movement of the voltage sensors, the presence of arginine as opposed to lysine residues enables a relatively long-range movement for the given electrostatic energy. More experimental and modeling studies on the interactions between the voltage sensor and the explicit lipid headgroups are warranted.

Although the ICK peptide toxins from scorpions and cone snails have been suggested to have evolved from a common ancestor gene, their relatively low sequence similarity ($<$30%) and the diverse functions are remarkable (9). Interestingly, unlike the other known ICK peptides, tachystatin B of horseshoe crab exhibits antimicrobial activity, which is likely to be mediated by the ICK motif (36). Spider ICK peptides, such as HaTx1 and GsMTx4, are structurally similar to those of scorpions, but there is still a large diversity even among the spider ICK peptides (9). From the example of HaTx1 and GsMTx4, we surmise that ICK peptides may generally have quite distinct ways of interaction with membranes, endowing variety to their functions. It is tempting to envisage that this variation may be related to the very subtle factors involving the flexibility of the lipids as well as the unique shapes of the peptides.

CONCLUSION

We carried out molecular dynamics simulation analyses of HaTx1 and GsMTx4 peptides, both belonging to the ICK peptide family, within DPPC and POPC membranes. For any combination of peptide and membrane, two binding modes were observed, namely, the shallow mode and the deep mode. In the shallow mode, all the positively charged residues interacted with the outer leaflet lipid, whereas in the deep mode the positively charged groups of K-8 and K-28 (in GsMTx4) and R-24 and K-26 (in HaTx1) interacted with carbonyl oxygen atoms of the inner leaflet lipids. For both toxins, our mean force measurement analyses showed that the deep binding mode is energetically more favorable than the shallow mode when a DPPC bilayer membrane was used. In contrast, when a POPC membrane was used, the two binding modes were energetically comparable for both toxins.

Therefore, the structure of the lipid acyl chains likely influences the locations and the dynamics of the toxins within biomembranes. Since our findings also show the difference in binding energy between the DPPC and POPC cases, it may be envisaged that the presence of ICK peptides may influence the local composition of lipids in the vicinity of the peptides. Inspired by the distinct behaviors of the toxins, we also compared the behavior of an arginine and a lysine residue within the DPPC membrane. The arginine residue generally showed smoother dynamics near the lipid carbonyl oxygen atoms than the lysine residue. This difference may partly explain the functional diversity of the members of the toxin family involving HaTx1 and GsMTx4. More analyses are necessary to gain insight into the relevance of these findings concerning the two binding modes to real biological membranes.

SUPPLEMENTARY MATERIAL

An online supplement to this article can be found by visiting BJ Online at http://www.biophysj.org.

We thank the reviewers and Dr. H. Cole for their valuable comments.

REFERENCES

1. Sachs, F., and C. E. Morris. 1998. Mechanosensitive ion channels in nonspecialized cells. *In* Reviews of Physiology, Biochemistry and Pharmacology. M. P. Blaustein, R. Greger, H. Grunicke, R. Jahn, L. M. Mendell, A. Miyajima, D. Pette, G. Schultz, and M. Schweiger, editors. Springer, Berlin. 1–78.
2. Suchyna, T. M., J. H. Johnson, K. Hamer, J. F. Leykam, D. A. Gage, H. F. Clemo, C. M. Baumgarten, and F. Sachs. 2000. Identification of a peptide toxin from Grammostola spatulata spider venom that blocks cation-selective stretch-activated channels. *J. Gen. Physiol.* 115:583–598.
3. Bode, F., F. Sachs, and M. R. Franz. 2001. Tarantula peptide inhibits atrial fibrillation. *Nature.* 409:35–36.
4. Oswald, R. E., T. M. Suchyna, R. McFeeters, P. Gottlieb, and F. Sachs. 2002. Solution structure of peptide toxins that block mechanosensitive ion channels. *J. Biol. Chem.* 277:34443–34450.
5. Lee, S.-Y., and R. MacKinnon. 2004. A membrane-access mechanics of ion channel inhibition by voltage sensor toxins from spider venom. *Nature.* 430:232–235.
6. Wang, J. M., S. H. Roh, S. Kim, C. W. Lee, J. J. Kim, and K. J. Swartz. 2004. Molecular surface of tarantula toxins interacting with voltage sensors in Kv channels. *J. Gen. Physiol.* 123:455–467.
7. Middleton, R. E., V. A. Warren, R. L. Kraus, J. C. Hwang, C. J. Liu, G. Dai, R. M. Brochu, M. G. Kohler, Y. D. Gao, V. M. Garsky, M. J. Bogusky, J. T. Mehl, C. J. Cohen, and M. M. Smith. 2002. Two tarantula peptides inhibit activation of multiple sodium channels. *Biochemistry.* 41:14734–14747.
8. Escoubas, P., S. Diochot, M. L. Celerier, T. Nakajima, and M. Lazdunski. 2002. Novel tarantula toxins for subtypes of voltage-dependent potassium channels in the Kv2 and Kv4 subfamilies. *Mol. Pharmacol.* 62:48–57.
9. Zhu, S., H. Darbon, K. Dyason, F. Verdonck, and J. Tytgat. 2003. Evolutionary origin of inhibitor cysteine knot peptides. *FASEB J.* 17:1765–1767.
10. Takahashi, H., J. I. Kim, H. J. Min, K. Sato, K. J. Swartz, and I. Shimada. 2000. Solution structure of hanatoxin1, a gating modifier of voltage-dependent K(+) channels: common surface features of gating modifier toxins. *J. Mol. Biol.* 297:771–780.
11. Suchyna, T. M., S. E. Tape, R. E. Koeppe II, O. S. Andersen, F. Sachs, and P. A. Gottlieb. 2004. Bilayer-dependent inhibition of mechanosensitive channels by neuroactive peptide enantiomers. *Nature.* 430:235–240.
12. O'Connell, A. M., R. E. Koeppe II, and O. S. Andersen. 1990. Kinetics of gramicidin channel formation in lipid bilayers: transmembrane monomer association. *Science.* 250:1256–1259.
13. Berendsen, H. J. C. 1996. Bio-molecular dynamics comes of age. *Science.* 271:954–955.
14. Karplus, M. 2002. Molecular dynamics simulations of biomolecules. *Acc. Chem. Res.* 35:321–322.
15. Tieleman, D. P., S. J. Marrink, and H. J. C. Berendsen. 1997. A computer perspective of membranes: molecular dynamics studies of lipid bilayer systems. *Biochem. Biophys. Acta.* 1331:235–270.
16. Forrest, L. R., and M. S. Sansom. 2000. Membrane simulations: bigger and better? *Curr. Opin. Struct. Biol.* 10:174–181.
17. Hansson, T., C. Oostenbrink, and W. F. van Gunsteren. 2002. Molecular dynamics simulations. *Curr. Opin. Struct. Biol.* 12:190–196.
18. Shepherd, C. M., H. J. Vogel, and D. P. Tieleman. 2003. Interactions of the designed antimicrobial peptide MB21 and truncated dermaseptin S3 with lipid bilayers: molecular-dynamics simulations. *Biochem. J.* 370:233–243.
19. Ash, W. L., M. R. Zlomislic, E. O. Oloo, and D. P. Tieleman. 2004. Computer simulations of membrane proteins. *Biochem. Biophys. Acta.* 1666:158–189.
20. Gumbart, J., Y. Wang, A. Aksimentiev, E. Tajkhorshid, and K. Schulten. 2005. Molecular dynamics simulations of proteins in lipid bilayers. *Curr. Opin. Struct. Biol.* 15:423–431.
21. Nishizawa, M., and K. Nishizawa. 2006. Interaction between K^+ channel gate modifier hanatoxin and lipid bilayer membranes analyzed by molecular dynamics simulation. *Eur. Biophys. J.* 35:373–381.
22. Phillips, L. R., M. Milescu, Y. Li-Smerin, J. A. Mindell, J. I. Kim, and K. J. Swartz. 2005. Voltage-sensor activation with a tarantula toxin as cargo. *Nature.* 436:857–860.
23. Lindahl, E., B. Hess, and D. van der Spoel. 2001. GROMACS 3.0: a package for molecular simulation and trajectory analysis. *J. Mol. Mod.* 7:306–317.
24. Berendsen, H. J. C., D. van der Spoel, and R. van Drunen. 1995. GROMACS: a message-passing parallel molecular dynamics implementation. *Comput. Phys. Commun.* 91:43–56.
25. Tieleman, D. P., and H. J. C. Berendsen. 1996. Molecular dynamics simulations of fully hydrated DPPC with different macroscopic boundary conditions and parameters. *J. Chem. Phys.* 105:4871–4880.
26. van Gunsteren, W. F., P. Kruger, S. R. Billester, A. E. Mark, A. A. Eising, W. R. P. Scott, P. H. Huneberg, and I. G. Tironi. 1996. Biomolecular Simulation: The GROMOS96 Manual and User Guide. BIOMOS/Hochschuleverlag AG and der ETH, Zürich.
27. Berendsen, H. J. C., J. P. M. Postma, W. F. van Gunsteren, and J. Hermans. 1981. Intermolecular Forces, Interaction Models for Water in Relation to Protein Hydration. D. Reidel Publishing, Dordrecht, The Netherlands. 331–342.
28. Hess, B., H. Bekker, H. J. C. Berendsen, and J. G. E. M. Fraaije. 1997. LINCS: a linear constraint solver for molecular simulations. *J. Comput. Chem.* 18:1463–1472.
29. Darden, T., D. York, and L. Pedersen. 1993. Particle mesh Ewald: an *N*log(*N*) method for Ewald sums in large systems. *J. Chem. Phys.* 98:10089–10092.
30. Sagui, C., and T. A. Darden. 1999. Molecular dynamics simulations of biomolecules: long-range electrostatics effects. *Annu. Rev. Biophys. Biomol. Struct.* 28:155–179.
31. Berendsen, H. J. C., J. P. M. Postma, W. F. van Gunsteren, A. DiNola, and J. R. Haak. 1984. Molecular dynamics with coupling to an external bath. *J. Chem. Phys.* 81:3684–3690.
32. Humphery, W., A. Dalke, and K. Schulten. 1996. VMD: visual molecular dynamics. *J. Mol. Graph.* 14:33–38.
33. Swartz, K. J., and R. MacKinnon. 1995. An inhibitor of the Kv2.1 potassium channel isolated from the venom of a Chilean tarantula. *Neuron.* 15:941–949.
34. Jiang, Y., V. Ruta, J. Chan, A. Lee, and R. MacKinnon. 2003. The principle of gating charge movement in a voltage-dependent K^+ channel. *Nature.* 423:42–48.
35. Long, S. B., E. B. Campbell, and R. Mackinnon. 2005. Crystal structure of a mammalian voltage-dependent Shaker family K^+ channel. *Science.* 309:897–903.
36. Fujitani, N., T. Kohno, T. Nakahara, K. Takeya, T. Osaki, S. Kawabata, M. Mizuguchi, T. Aizawa, M. Demura, S. Nishimura, and K. Kawano. 2006. The solution structure of horseshoe crab antimicrobial tachystatin B with an inhibitory cystine-knot motif. *Proc. 20th IUBMB International Congress of Biochemistry and Molecular Biology and 11th FAOBMB Congress.* http://www.congre.co.jp/iubmb.